Food Sci Biotechnol (2021) 30(8):1087–1096
https://doi.org/10.1007/s10068-021-00949-1

RESEARCH ARTICLE

Evaluation of infrared assisted freeze drying for strawberry snacks: drying kinetics, energy efficiency and quality attributes

Su Wang Kang[1] · Jeong Hyeon Hwang[1] · Kang Hyun Chung[1] · Sung Hee Park[1]

Received: 15 April 2021 / Revised: 5 July 2021 / Accepted: 12 July 2021 / Published online: 28 July 2021

Abstract Feasibility of infrared assisted freeze drying (IRAFD) was evaluated for production of the strawberry snacks. Infrared (IR) radiation provided the driving force of ice sublimation during freeze drying (FD). Different IRAFD conditions were tested, including the continuous IRAFD-1.6 kW/m^2 and IRAFD-1.6 kW/m^2 at different weight reductions (20%, 40%, and 60%). Conventional FD had a total drying time of 691 ± 19 min, whereas continuous IRAFD significantly reduced the drying time to 309 ± 32 min. Continuous IRAFD also reduced the amount of consumed electrical energy by 42% compared to that of FD. A long duration of IR radiation produced a soft texture in the snacks. Drying kinetics were analyzed using various models, including the Page model, exponential model, and Henderson and Pabis model. The Page model provided the best fit to the experimental drying curve. This study showed the potential of IRAFD in producing value-added fruit snacks with good textural quality and efficient use of energy.

Keywords Infrared Assisted Freeze Drying · Strawberry · Texture · Energy · Rapid

✉ Sung Hee Park
sunghpark@seoultech.ac.kr

Su Wang Kang
swkang415@seoultech.ac.kr

Jeong Hyeon Hwang
jeonghh@seoultech.ac.kr

Kang Hyun Chung
carl@seoultech.ac.kr

[1] Department of Food Science and Technology, Seoul National University of Science and Technology, Seoul 01811, Republic of Korea

List of symbols

a, k	Drying constant of model
D_{eff}	Diffusion coefficient (m^2/min)
E	Energy (kJ/m^2)
I	Current (A)
L	Thickness of sample (mm)
M	Dry basis moisture content at arbitrary time
M_0	Initial moisture content
MR	Moisture ratio (dimensionless)
N	Shape factor for page model
t	Time (min, s)
V	Voltage (V)
W	Weight (kg)

Subscript

f	Final
FD	Freeze drying
i	Initial
$IRAFD$	Infrared assisted freeze drying
ris	Radiant energy
t	Time
tis	Total energy
vis	Vacuum energy

Introduction

Strawberry (*Fragaria* × *ananassa*) is a popularly consumed fruit with desirable sensory properties (taste, color) and high nutritional value, consisting of vitamins, minerals, flavonoids, anthocyanins, proteins, and phenolic compounds (Chu et al., 2020; Temiz and Özdemir, 2021; Van de Velde et al., 2013). Strawberries have a very short shelf life and senescent period due to their susceptibility to mechanical injury, excessive softening of texture,

physiological disorders, and infection caused by several pathogens that can rapidly reduce the quality of fruit, and these pose a challenge in the marketing of the fruit (Colussi et al., 2021; Guerreiro et al., 2015; Gol et al., 2013). An appropriate storage technique for strawberries should aim to minimize any sensorial and nutritional loss. Dehydration is commonly used to extend the shelf life of fruits by reducing the moisture content (Zhang et al., 2020b), and freeze drying (FD) is popularly used for the dehydration of fruits and vegetables because it preserves the original taste, flavor, color, and nutritional qualities. However, FD is a time- and energy-intensive process since ice sublimation takes a long time, as it requires deep freezing and a low operating pressure (Liu et al., 2020; Zhang et al., 2006). Recently, various technologies such as infrared radiation, microwave heating, and ultrasound vibration are being used in combination with FD (Colucci et al., 2018; Jiang et al., 2017; Khampakool et al., 2019; Liu et al., 2020; Merone et al., 2020; Wang et al., 2010; Wu et al., 2019a, 2019b; Zhang et al., 2020a). Of these, infrared assisted freeze drying (IRAFD) has been widely studied for the rapid FD of fruits, vegetables, and insect products (Khampakool et al., 2019, 2020; Liu et al., 2020; Wu et al., 2019a). In the IRAFD, infrared (IR) radiation provides radiant energy for ice sublimation, which is essential for FD (Khampakool et al., 2019; Liu et al., 2020; Wu et al., 2019a). IR drying is considered a promising method for drying food products with high moisture content; IR energy penetrates materials and is then converted to heat (Huang et al., 2021). IR radiation works according to the principle of electromagnetic radiation, which states that wavelengths between 0.78 and 1000 μm have both spectral and directional dependence (Pawar and Pratape, 2017). IRAFD is advantageous as it is energy efficient and reduces the amount of thermal energy required for drying. In this study, IRAFD was investigated for the rapid FD of strawberries. Freeze-dried strawberry slices are popularly used for fruit snacks for their attractive taste, crispy texture, and high nutritional value (Ciurzyńska et al., 2020). Consumer demand for fruit snacks has recently increased because of the positive health effects associated with the intake of nutrients and phytochemicals (Potter et al., 2013; Roe et al., 2013; Yeganehzad et al., 2020). These so-called fruit and vegetable "healthy snacks" are made of dried fruits and vegetables (Ciurzyńska et al., 2020).

Although there have been various studies on the FD of strawberries (Agnieszk and Andrzej, 2010; Zhang et al., 2020b), to the best of our knowledge, IRAFD has not been used in the production strawberry snacks. This study aimed to investigate the potential application of IRAFD to produce a shelf-stable strawberry snacks and determine the drying kinetics, energy efficiency, and quality attributes of IRAFD in the production of strawberry snacks.

Materials and methods

Strawberry sample preparation

Strawberries were purchased from a local market (Seoul, Korea), washed, and vertically sliced into 5 mm-thick discs. K-type thermocouple (Ø 0.25 mm, Omega Engineering, Stamford, CT, USA) was inserted into the geometric center of a representative sample in each batch (8–10 samples, 50 ± 2 g). It was used for temperature monitoring and process control of the IRAFD. Sliced samples were frozen at −50 °C in a deep freezer for 24 h and stored until further use within two months. The initial moisture content (M_i) of strawberry samples was estimated to be 0.89 by oven drying at 105 °C for 24 h.

IRAFD system

IRAFD system of this study was customized in a previous study (Khampakool et al., 2019). IRAFD system consisted of a cylindrical stainless steel (STS 316) chamber (inner diameter: 290 mm, height: 400 mm), a condenser at −100 °C, a near-infrared (NIR) lamp (E27 ES, Philips Lighting, Eindhoven, Netherland), a vacuum pump (JBA00089, WSA Motor Inc., Hanam, Korea), a data acquisition system (DAQ, 34972A, Keysight, Santa Clara, CA, USA), and a digital balance (CB-300, A&D, Seoul, Korea). IR radiation is usually classified as near-infrared (NIR, 0.75–2 μm), mid-infrared (MIR, 2–4 μm), or far-infrared (FIR, 4–1000 μm) (Huang et al., 2021; Jain and Pathare, 2004). Far-infrared radiation is suitable for drying thin layers, while near-infrared radiation is suitable for drying thicker bodies (Sakare et al., 2020). In this study, a NIR lamp was selected to dry the 5 mm-thick samples. The NIR lamp inside the vacuum chamber provided radiant energy at a distance of 150 mm from the samples to drive ice sublimation. The NIR intensity was adjusted based on the radiation initiation time. The detailed procedure for NIR intensity control is described in the following section for IRAFD treatment. Weight changes in the sample were measured and recorded every 30 s using a digital balance and an RS-232 communication cable. The sample temperature and electrical energy consumption (current and voltage) of the NIR lamp, which are important for process control, drying kinetics, and energy efficiency of IRAFD, were also measured and recorded every 30 s using a DAQ. The electrical energy consumption of the condenser and vacuum pump was measured using an electrical energy meter (SJPM-C16, SEOJUN ELECTIC, Seoul).

IRAFD treatment

Frozen strawberries (50 ± 2 g, 8–10 discs) were placed on a wire mesh tray (screen opening: 11.3 × 11.3 mm, total size: 160 × 160 mm). They were mounted on a digital balance equipped with an RS-232 communication cable for data recording. Five different drying treatments were tested in this study, thus, diversifying the IR initiation time. These were: (1) FD; (2) Continuous IRAFD-1.6 kW/m^2; (3) IRAFD-1.6 kW/m^2 at 20% WR; (4) IRAFD-1.6 kW/m^2 at 40% WR; (5) IRAFD-1.6 kW/m^2 at 60% WR. In the FD trial, frozen strawberry samples were freeze-dried without IR radiation at a vacuum of 6.67 Pa and condenser temperature of − 100 °C. IR radiation energy (1.6 kW/m^2) was provided when sample weight was reduced by 20, 40 and 60% during FD for IRAFD-1.6 kW/m^2 at 20% WR, IRAFD-1.6 kW/m^2 at 40% WR, and IRAFD-1.6 kW/m^2 at 60% WR trials, respectively. Continuous IRAFD-1.6 kW/m^2 treatment involved the continuous exposure of samples to IR radiant energy of 1.6 kW/m^2 during the entire FD period. All drying treatments were performed until the final moisture content (M_f) was 0.11, and the final temperature was 25 °C. The sample temperature was controlled using a proportional-integral-derivative (PID) controller (ITC-100VH, INK BIRD, Shenzhen, China).

Radiant energy

The radiant energy of IR had a significant role in determining the drying rate and energy efficiency of IRAFD because it drives ice sublimation. The total energy for ice sublimation (E_{tis}) is the sum of the vacuum energy (E_{vis}) and radiant energy (E_{ris}) in IRAFD (Khampakool et al., 2019, 2020) and is expressed as follows:

$$E_{tis} = E_{vis} + E_{ris} \quad (1)$$

where E_{tis} is the total energy, E_{vis} is the vacuum energy, and E_{ris} is the radiant energy (J).

The total energy (E_{tis}) of ice sublimation can be estimated as a function of the sample weight (W), initial moisture content (M_i), final moisture content (M_f), and latent heat of ice sublimation (L_s) (Khampakool et al., 2019, 2020).

$$E_{tis} = W \times \left(M_i - M_f\right) \times L_s \quad (2)$$

where E_{tis} is the total energy of ice sublimation (J), W is the sample weight (kg), M_i is the initial moisture content, M_f is the final moisture content, and L_s is the latent heat for ice sublimation (Khampakool et al., 2019, 2020).

M_i and M_f were determined to be 0.89 and 0.11, respectively. The latent heat of ice sublimation is 2.834 × 10^3 kJ·kg^{-1} (Khampakool et al., 2019, 2020; Zdunkowski and Bott, 2004). The estimated E_{tis} of strawberries was calculated to be 110,526 J. In FD, E_{tis} and E_{vis} were identical because FD used only vacuum energy for ice sublimation (Khampakool et al., 2019, 2020). In the IRAFD trials, vacuum energy ($E_{vis,\ IRAFD}$) varies as a function of the total energy for ice sublimation (E_{tis}), FD time (t_{FD}), and IRAFD time (t_{IRAFD}), as suggested in our previous studies (Khampakool et al., 2019, 2020).

$$E_{vis,IRAFD} = E_{tis} \times \frac{t_{IRAFD}}{t_{FD}} \quad (3)$$

where $E_{vis.IRAFD}$ is the vacuum energy of IRAFD (J), t_{IRAFD} is the drying time for IRAFD (min), and t_{FD} is the drying time for FD (min).

Eventually, the radiant energy of IRAFD ($E_{ris,IRAFD}$) is estimated by excluding $E_{vis.IRAFD}$ from E_{tis} as follows (Khampakool et al., 2019, 2020).

$$E_{ris,IRAFD} = E_{tis} - E_{vis,IRAFD} \quad (4)$$

where $E_{ris\ IRAFD}$ is the radiant energy of IRAFD (J), E_{tis} is the total energy, and $E_{vis\ IRAFD}$ is the vacuum energy of IRAFD (J).

Moisture ration (*MR*)

The moisture ratio (*MR*) is a ratio of the change in moisture content and time and was calculated as follows:

$$MR = \frac{M_t - M_f}{M_i - M_f} \quad (5)$$

where M_t is the moisture content at an arbitrary time, M_i is the initial moisture content, and M_f is the final moisture content of each treatment. The drying kinetics of each dried strawberry sample used four different models, including the Page model, exponential model, Henderson and Pabis model and the simplified diffusion model. Previous studies have successfully demonstrated the drying kinetics of agricultural products using these models (Azeez et al., 2019; Dissa et al., 2008; Khampakool et al., 2019; Lin et al., 2005; Charmongkolpradit and Luampon, 2017).

Drying kinetics

The exponential model

The exponential model is the most simplified drying model that is proposed to simulate the drying curves of foods (Senadeera et al., 2003; Simal et al., 2005), as shown in Eq. (6). It is a representative empirical model describing thin-layer drying of agricultural foods (Lin et al., 2005).

$$MR = \exp(-k \cdot t) \quad (6)$$

where MR is the moisture ratio, k is the drying constant (min^{-1}), and t is the time (min).

The page model

The Page model is derived from the exponential model, wherein it overcomes the defect of the exponential model by adopting the exponent shape factor "*N*" (Simal et al., 2005; Akpinar et al., 2003; Iguaz et al., 2003).

$$MR = \exp(-k \cdot t^N) \tag{7}$$

where *MR* is the moisture ratio, *k* is the drying constant, *t* is time (min), and *N* is the shape factor.

Henderson and Pabis model

The Henderson and Pabis model simplifies the first term of the series solution of Fick's second law. This model explains the drying rate at the beginning of the drying process; however, it shows the discrepancy of fitting at the last stage of drying (Dissa et al., 2008).

$$MR = a \cdot \exp(-k \cdot t) \tag{8}$$

where *MR* is the moisture ratio, *a* and *b* are the drying constants, and *t* is the time (min).

The simplified diffusion model

The simplified diffusion model is theoretically based on Fick's diffusion model which estimate the effective moisture diffusivity in the drying of fruit and vegetable (Khampakool et al., 2019; Lin et al., 2005; Maskan et al., 2002)

$$MR = \frac{M}{M_0} = \frac{8}{\pi^2} \times \exp\left[-\pi^2 \frac{D_{eff} t}{4L^2}\right] \tag{9}$$

where *MR* is moisture ratio, *M* is moisture content at an arbitrary time (t, min), M_0 is initial moisture content, D_{eff} is diffusion coefficient (m^2/min), *L* is thickness of the sample (mm), and *t* is time (min).

Texture analysis

For texture analysis, the hardness of dried strawberry samples was tested using a TA-XT texture analyzer (Texture Technology Corp., Brewster, NY, USA). The texture analysis parameters were obtained by modifying parameters of a previous study (Zhang et al., 2020b). The dried sample was placed in an acryl tube (diameter: 15 mm, height: 13 mm). A cylindrical probe with a diameter of 2 mm (P/2, 2 mm Ø, cylinder, stainless steel) broke down and passed through 40% of the sample thickness with a pre-test speed of 5 mm/s, test speed of 2 mm/s, and post-test speed of 5 mm/s.

Microstructure analysis

Microstructure analysis of dried strawberry samples was conducted using a scanning electron microscope (SEM, JSM-7900F, JEOL INC, MA USA), as described in our previous study (Khampakool et al., 2019). The dried sample discs were sliced across the cross-sectional surface and coated with platinum using an ion coater (Cressington Sputter Coater 108 Auto., TED PELLA, INC. USA, Canada) under vacuum (0.1 Pa). SEM image analysis was conducted at an acceleration voltage of 5 kV. The final microscopic image was captured at a 1024 × 960 pixel resolution at 60 × magnification.

Color measurement

A colorimeter (CR-10, Konica Moinolta Sensing Inc., Sakai, Osaka, Japan) was used to measure the color of the dried strawberries. These were designated as *L** (brightness), *a** (redness), and *b** (yellowness), respectively. The total color difference (ΔE) was calculated to estimate the overall color change as compared to those of raw strawberries, as shown in Eq. (10).

$$\Delta E = \sqrt{(L* - L_0)^2 + (a* - a_0)^2 + (b* - b_0)^2} \tag{10}$$

Electrical energy consumption

The drying process has an intensive energy demand, accounting for 20–25% of the total energy usage of the food industry (Kumar et al., 2014; Merone et al., 2020). Electrical energy consumption of IRAFD includes the energy consumed by the condenser, vacuum pump, and IR lamp. An electrical energy meter (SJPM-C16, SEOJUN ELECTIC, Seoul) was used to estimate the energy consumption of the condenser and vacuum pump in the IRAFD. DAQ system was used to record the voltage and current usage of the NIR lamp. Electrical energy consumption rate (Watt, J/s) of the IR lamp was calculated using Ohm's law. Electrical energy consumption of the IR lamp (J) was estimated by integration of electrical energy consumption rate to the drying time, as suggested in our previous studies (Khampakool et al. 2019, 2020).

$$E_{IR} = \int_{t_i}^{t_f} I \cdot V dt \tag{11}$$

where E_{IR} is the energy consumed by the IR lamp (J), *I* is the current (A), *V* is the voltage (V), and *t* is the drying time (s). Mathematical integration of Eq. (11) was conducted using trapezoidal function of MATLAB software (Version 2018b, Mathworks INC, MA, USA) as previously

proposed (Khampakool et al., 2020; Park and Jo, 2019; Park et al., 2014).

Statistical analysis

All IRAFD and FD treatments were performed in triplicates. Experimental data was analyzed using a statistical analysis system program (SAS, version 9.1.3, SAS Institute, Cary, NC, USA). Multiple comparisons of mean values were conducted using the analysis of variance and Fisher's least significant difference method at a confidence interval of 95% ($p < 0.05$).

Result and discussion

Moisture ratio, temperature profiles, and drying rate

Changes in the moisture ratio and temperature profiles of the dried strawberry samples are shown in Fig. 1. FD showed the slowest reduction in moisture and the longest total drying time of 691 ± 19 min (Table 1) as compared to the other methods. The temperature of the FD sample did not significantly change until after 300 min, after which it gradually increased to 14 °C. In this study, thermocouple was inserted into geometric center of the sample. Once surface ice was primarily sublimed at the surface of sample; thus, internal temperature was not dramatically changed until surface ice was sublimed. All IRAFD trials reduced the total drying time and exhibited a steeper moisture reduction curve as compared to FD. The drying time for the IRAFD trials was influenced by the initial application time of the IR radiation. For IRAFD-1.6 kW/m^2 at 60% WR, IR radiation was initiated at 332 ± 7 min when the sample weight was reduced by 60%, and then sample temperature drastically increased from 370 ± 30 min. IR radiation did not induce an immediate change in the sample temperature until the IR energy and heat penetrated to the center. IRAFD-1.6 kW/m^2 at 60% WR showed a more rapid drying rate of 5.7 ± 0.1 g/h with an application of 28.5 ± 3.4 kJ radiant energy, suggesting that the enhanced drying rate during IRAFD corresponds to increased radiant energy (Khampakool et al., 2019, 2020). During continuous IRAFD-1.6 kW/m^2, IR was applied at the beginning of FD, and a more rapid drying rate of 9.2 ± 0.2 g/h was possible since it has the highest radiant energy (59.4 ± 1.8 kJ) compared to the other IRAFD methods (Khampakool et al., 2019, 2020). With respect to the drying rate, earlier application and longer duration of IR reduces the drying time. However, it is important to note that excessive IR energy and heat generation can theoretically induce a collapse phenomenon during FD (Wu et al., 2019a).

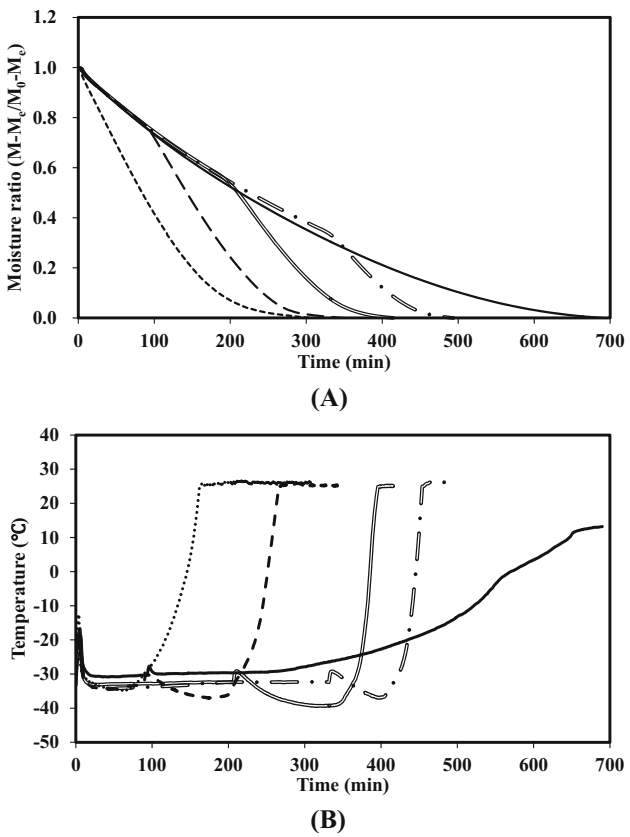

Fig. 1 (**A**) Moisture ratio and (**B**) temperature profiles of strawberry during FD and different IRAFD trials (black line: FD, double gray line: IRAFD-1.6 kW/m^2 at 60% WR, single gray line: IRAFD-1.6 kW/m^2 at 40% WR, black long dash line: IRAFD-1.6 kW/m^2 at 20% WR, black small dash line: continuous IRAFD-1.6 kW/m^2). (WR: weight reduction)

Drying kinetics

Table 2 presents the coefficients of estimated drying kinetics which include the Exponential model, Page model, Henderson and Pabis model and the simplified diffusion model. In the accuracy of model fitting, Page model showed the best fit with highest coefficient of determination (COD, R^2) values followed by Henderson and Pabis model, exponential model and the simplified diffusion model. In this study, the drying curve of moisture ratio was influenced by the application time of IR radiation; thus, moisture ratio profiles showed non-linear curves. The Page model considers both k and shape factor (N) which could best explain the non-linear drying curve.

In the exponential model, FD showed the drying constant (k, min^{-1}) of 0.00376 (Table 2). k values were found to gradually increase with an increase in IR radiation time from IRAFD-1.6 kW/m^2 at 40% WR. k value increments indicated a shorter drying time with IR radiation and

Table 1 Drying time, drying rate, vacuum energy (J), and radiant energy (E_{rd}, J) of FD and different IRAFD trials for dried strawberry

Methods	Total drying time (min)	IR radiation application time (min)	Temperature increased time (min)	IR radiation time (min)	Drying rate (g/h)	Vacuum energy (kJ)	Radiant energy (E_{rd}, kJ)
FD	691 ± 19[a]				4.0 ± 0.2[e]	114.0 ± 7.3[a]	0.0 ± 0.0[e]
IRAFD-1.6 kW/m^2 at 60% WR	495 ± 19[b]	332 ± 7[a]	370 ± 30[a]	162 ± 19[c]	5.7 ± 0.1[d]	85.4 ± 3.4[b]	28.5 ± 3.4[d]
IRAFD-1.6 kW/m^2 at 40% WR	416 ± 27[c]	197 ± 9[b]	273 ± 61[b]	219 ± 26[b]	6.9 ± 0.1[c]	71.8 ± 0.9[c]	42.1 ± 0.9[c]
IRAFD-1.6 kW/m^2 at 20% WR	351 ± 6[d]	90 ± 3[c]	215 ± 22[b]	261 ± 8[b]	8.0 ± 0.1[b]	60.5 ± 2.2[d]	53.4 ± 2.2[b]
Continuous IRAFD-1.6 kW/m^2	309 ± 32[e]	0 ± 0[d]	97 ± 24[c]	309 ± 32[a]	9.2 ± 0.2[a]	54.5 ± 1.8[e]	59.4 ± 1.8[a]

[a–e]Means (± SD) with a different letter in the same column are significantly different at $p < 0.05$

WR weight reduction

generation of radiant energy for ice sublimation. The exponential model showed a relatively low R^2 values as compared to the Page model.

k values of the Page model showed different trends compared to those of the other models. Except for continuous IRAFD-1.6 kW/m^2, other IRAFD trials had lower k values than that of FD. In this study, the Page model was more dependent on N than on k. The Page model suitably explains downward concave ($N > 1$) and upward concave ($N < 1$) drying curves (Khampakool et al., 2019, 2020; Park et al., 2013). IRAFD-1.6 kW/m^2 at 20%, 40%, and 60% initially showed a linear drying curve and then converted to a downward concave drying curve after IR radiation. The IR application time had a significant effect on the drying curves. Previous studies have reported that the Page model accurately describes the drying kinetics of agricultural products using both k and N (Chawla et al., 2008; Gaware et al., 2010; Krokida and Philippopoulos, 2005; Lopez-Quiroga et al., 2020). The Page model showed the highest R^2 values among the tested models, as shown in Table 2.

The Henderson and Pabis model showed relatively lower R^2 values in IRAFD-1.6 kW/m^2 at 60, 40 and 20% WR. This model predicts the drying rate at the beginning of the drying process, but it is less efficient in the final stages of the process (Dissa et al., 2008; Henderson and Pabis, 1961). In this study, IR radiation influenced the drying process, and the Henderson and Pabis model could not appropriately explain the IR radiation time.

The simplified diffusion model showed the lowest R^2 values among tested drying kinetics. In case of simplified diffusion model, it considers the changes in the sample size such as thickness (L) of the sample; however, in our study, thickness of sample was not changed during IRAFD and FD process. This might result in the lowest R^2 of this model.

Microstructure

The SEM images of the dried strawberry samples are shown in Fig. 2. FD led to the generation of relatively small pores (0.0097–0.0134 mm^2) as compared to those (0.0125–0.0417 mm^2) in the IRAFD samples. IRAFD-1.6 kW/m^2 at 60% led to larger pores than FD, and the pore sizes were not uniform. There was no clear difference between the SEM images of samples dried using IRAFD-1.6 kW/m^2 at 60%, IRAFD-1.6 kW/m^2 at 40% and IRAFD-1.6 kW/m^2 at 20%. Continuous IRAFD, wherein IR radiation is initiated at an early stage, led to the generation of the largest (0.0329 ± 0.0072 mm^2) and most uniform pores. Khampakool et al. (2019) reported that continuous IRAFD led to generation of the largest pores in banana, and these can entrap air. Previous IRAFD studies proved that IR radiation provides energy for rapid heating, causing water vapor to diffuse across cellular walls and create large pores (Jamradloedluk et al., 2007; Khampakool et al., 2019; Shih et al., 2008). Monteiro et al. (2018) reported that volumetric heating also caused the formation of larger pores and faster vapor production, when microwave was applied during FD of pumpkin slices. In this study, no visual collapse was observed during the FD and IRAFD trials because the IR power was appropriately controlled in the preliminary experiment.

Texture

The hardness of FD-and IRAFD-treated strawberry samples were compared (Table 3). FD showed the highest

Table 2 Coefficient of estimated model fitting of FD and different IRAFD trials for dried strawberry

Model	Method	a	k (min^{-1})	$D_{eff} \times 10^{-6}$ (m^2/min)	N	R^2
Exponential model $MR = \exp(-k \cdot t)$	FD		0.00376			0.971
	IRAFD-1.6 kW/m^2 at 60% WR		0.00370			0.915
	IRAFD-1.6 kW/m^2 at 40% WR		0.00445			0.869
	IRAFD-1.6 kW/m^2 at 20% WR		0.00621			0.874
	Continuous IRAFD-1.6 kW/m^2		0.00997			0.962
Page model $MR = \exp(-k \cdot t^N)$	FD		0.00075		1.281	0.992
	IRAFD-1.6 kW/m^2 at 60% WR		0.00030		1.451	0.959
	IRAFD-1.6 kW/m^2 at 40% WR		0.00004		1.872	0.969
	IRAFD-1.6 kW/m^2 at 20% WR		0.00003		2.058	0.994
	Continuous IRAFD-1.6 kW/m^2		0.00141		1.409	0.997
Henderson and Pabis model $MR = a \cdot \exp(-k \cdot t)$	FD	1.087	0.00409			0.979
	IRAFD-1.6 kW/m^2 at 60% WR	1.100	0.00412			0.928
	IRAFD-1.6 kW/m^2 at 40% WR	1.174	0.00528			0.901
	IRAFD-1.6 kW/m^2 at 20% WR	1.241	0.00764			0.921
	Continuous IRAFD-1.6 kW/m^2	1.146	0.01132			0.978
The simplified diffusion model $MR = (8/\pi^2)\exp[(-\pi^2/L^2) \cdot D \cdot t]$	FD			0.008		0.893
	IRAFD-1.6 kW/m^2 at 60% WR			0.007		0.807
	IRAFD-1.6 kW/m^2 at 40% WR			0.009		0.752
	IRAFD-1.6 kW/m^2 at 20% WR			0.013		0.761
	Continuous IRAFD-1.6 kW/m^2			0.021		0.884

hardness of 1.08 ± 0.06 N, while all the IRAFD treatments decreased the hardness of dried strawberries. Longer exposure to IR light decreased the hardness, and the lowest hardness of 0.60 ± 0.05 N was found in samples dried by continuous IRAFD-1.6 kW/m^2. For example, large pore size (0.0329 ± 0.0072 mm^2) of continuous IRAFD −1.6 kW/m^2 had low hardness of 0.60 ± 0.05 N. Whereas, when pore size was decreased to 0.0114 ± 0.0014 mm^2 at the FD treatment, hardness increased to 1.08 ± 0.06 N.

The texture of dried food is closely related to its microstructure. As mentioned above, IR radiation induced a larger pore size and entrapped air in dried strawberries by triggering water vapor diffusion through the cellular wall. This would result in a lower hardness and enhanced crispness of the IRAFD samples. The crispness was mainly related to crust formation and structural changes. Previously, it has been shown that IR radiation during FD formed a modest crust and created a large porous structure in the central region of dried banana, resulting in a crispy product (Pan et al., 2008). The so-called fruit and vegetable "healthy snacks" are made from ingredients such as dried fruits and vegetables (Ciurzyńska et al., 2020). This

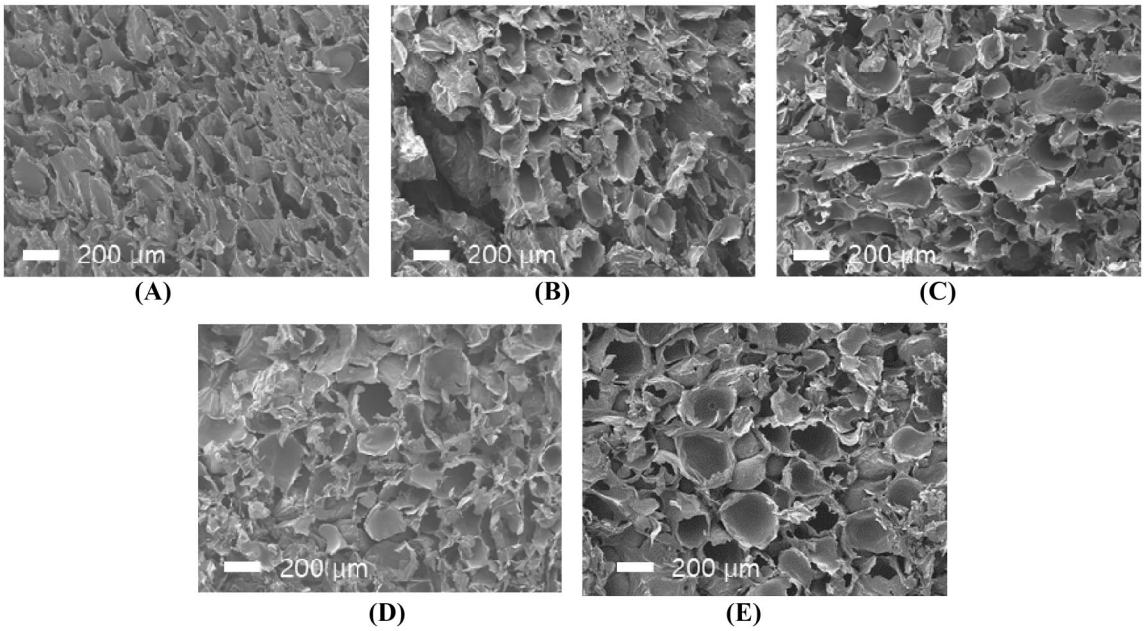

Fig. 2 SEM of cross section of dried strawberry during FD and different IRAFD trial: (**A**) FD, (**B**) IRAFD-1.6 kW/m^2 at 60% WR, (**C**) IRAFD-1.6 kW/m^2 at 40% WR, and (**D**) IRAFD-1.6 kW/m^2 at 20% WR (**E**) continuous IRAFD-1.6 kW/m^2

Table 3 Effect of FD and different IRAFD trials hardness and color of dried strawberry

Methods	Hardness (N)	L^*	a^*	b^*	ΔE
Raw		31.0 ± 1.2^{b}	49.7 ± 0.9^{a}	27.7 ± 1.8^{a}	
FD	1.08 ± 0.06^{a}	34.4 ± 1.6^{a}	46.0 ± 1.3^{ab}	19.0 ± 0.2^{c}	10.2 ± 0.4^{a}
IRAFD-1.6 kW/m^2 at 60% WR	0.82 ± 0.07^{b}	31.6 ± 2.9^{ab}	41.9 ± 4.4^{c}	18.9 ± 0.8^{c}	12.3 ± 3.2^{a}
IRAFD-1.6 kW/m^2 at 40% WR	0.77 ± 0.05^{c}	31.7 ± 0.9^{ab}	44.3 ± 0.8^{bc}	21.3 ± 0.9^{b}	8.5 ± 1.1^{a}
IRAFD-1.6 kW/m^2 at 20% WR	0.76 ± 0.02^{d}	30.9 ± 0.9^{b}	42.1 ± 2.1^{bc}	18.9 ± 1.2^{c}	11.7 ± 2.2^{a}
Continuous IRAFD-1.6 kW/m^2	0.60 ± 0.05^{e}	33.6 ± 1.6^{ab}	43.5 ± 0.8^{bc}	19.0 ± 1.2^{c}	11.1 ± 0.8^{a}

$^{a–e}$Means (± SD) with a different letter in the same column are significantly different at $p < 0.05$

WR weight reduction

study demonstrated the potential of IRAFD to improve the textural qualities of dried fruit snacks.

Color

The color value of strawberries dries using FD and IRAFD treatment was determined (Table 3). Raw strawberry had the L^*, a^* and b^* values of 31.0 ± 1.2, 49.7 ± 0.9, 27.7 ± 1.8. FD increased the L^* value; whereas, a^* and b^* values were decreased after FD treatment. FD showed the L^*, a^* and b^* values as 34.4 ± 1.6, 46.0 ± 1.3, 19.0 ± 0.2, respectively. L^* value of IRAFD samples ranged from 31.6 to 33.6, while a^* value of IRAFD samples ranged from 41.9 to 46.0, and b^* value of IRAFD samples ranged from 18.9 to 21.3. There was no significant difference among color values determined for the different drying methods. Total color difference (ΔE) value was not significantly different among FD and IRAFD trials ($p > 0.05$). Previous study also demonstrated the IR radiation during FD did not influence the color value of fruit products (Khampakool et al., 2019). In this study, IR radiation did not induce any discoloration of dried strawberries.

Electrical energy consumption

The electrical energy consumption of the FD and IRAFD methods was determined (Table 4). FD consumed a total electrical energy of 23.49 × 10^3 kJ. All IRAFD trials saved electrical energy compared to that of FD. Continuous IRAFD-1.6 kW/m^2 consumed the least electrical energy of 13.63 × 10^3 kJ because it reduced the drying time by 65%

Table 4 Electrical energy consumption of FD and different IRAFD trials for dried strawberry

Methods	Vacuum pump ($\times 10^3$ kJ)	Condenser ($\times 10^3$ kJ)	IR lamp ($\times 10^3$ kJ)	Total ($\times 10^3$ kJ)
FD	9.83 ± 0.40^{a}	13.66 ± 4.88^{a}	-	23.49 ± 5.17^{a}
IRAFD-1.6 kW/m^2 at 60% WR	7.52 ± 0.09^{b}	13.32 ± 0.044^{ab}	0.35 ± 0.07^{b}	20.85 ± 0.08^{ab}
IRAFD-1.6 kW/m^2 at 40% WR	6.27 ± 0.05^{c}	11.52 ± 0.23^{abc}	0.44 ± 0.06^{ab}	17.80 ± 0.20^{bc}
IRAFD-1.6 kW/m^2 at 20% WR	5.16 ± 0.26^{d}	9.38 ± 0.40^{bc}	0.48 ± 0.03^{a}	14.55 ± 0.26^{c}
Continuous IRAFD-1.6 kW/m^2	4.64 ± 0.08^{e}	8.98 ± 0.10^{c}	0.54 ± 0.10^{a}	13.63 ± 0.09^{c}

[a–e]Means (± SD) with a different letter in the same column are significantly different at $p < 0.05$

WR weight reduction

compared to that of FD. In continuous IRAFD-1.6 kW/m^2, the condenser spent most of the electrical energy at 8.98×10^3 kJ, followed by the vacuum pump at 4.64×10^3 kJ. Although the IR lamp was continuously on during continuous IRAFD, it consumed very low electrical energy (0.54×10^3 kJ). IR drying technology has the advantages of good energy efficiency, rapid drying, uniform heating, superior quality of the final products, and low energy costs (Huang et al., 2021). IR radiation efficiently provided radiant energy for ice sublimation and subsequent rapid drying with minimized electrical energy consumption. Our study shows the potential of IRAFD for energy-efficient drying technology. The results will be useful for the production of value-added fruit snacks.

Acknowledgements This study was supported by the Research Program funded by the SeoulTech(Seoul National University of Science and Technology).

Declarations

Conflict of interest The authors declare that they have no conflict of interests.

References

Agnieszk C, Andrzej L. Rehydration and sorption properties of osmotically pretreated freeze-dried strawberries. Journal of Food Engineering 97: 267-274 (2010)

Akpinar E, Midilli A., Bicer Y. Single layer drying behaviour of potato slices in a convective cyclone dryer and mathematical modeling. Energy Conversion and Management 44: 1689-1705 (2003)

Azeez L, Adebisi SA, Oyedji AO, Adetoro RO, Tajani KO. Bioactive compounds' contents, drying kinetics and mathematical modelling of tomato slices influenced by drying temperatures and time. Journal of the Saudi Society of Agricultural Sciences 18: 120-126 (2019)

Charmongkolpradit S, Luampon R. Study of thin layer drying model for cassava pulp. Energy Procedia 138: 354-359 (2017)

Chawla C, Kaur D, Oberoi DPS, Sogi DS. Drying characteristics, sorption isotherms, and lycopene retention of tomato pulp. Drying Technology 26: 1257-1264 (2008)

Chu Y, Gao C, Liu X, Zhang N, Xu T, Feng X,Yang Y, Shen X, Tang X. Improvement of storage quality of strawberries by pullulan coatings incorporated with cinnamon essential oil nanoemulsion. LWT - Food Science and Technology 122: 109054 (2020)

Ciurzyńska A, Marczak W, Lenart A, Janowicz M. Production of innovative freeze-dried vegetable snack with hydrocolloids in terms of technological process and carbon footprint calculation. Food Hydrocolloids 108: 105993 (2020)

Colucci D, Fissore D, Rossello C, Carcel JA. On the effect of ultrasound-assisted atmospheric freeze-drying on the antioxidant properties of eggplant. Food Research International 106: 580-588 (2018)

Colussi R, Ferreira da Silva WM, Biduski B, El Halal SLM, Zavareze EDR, Dias ARG. Postharvest quality and antioxidant activity extension of strawberry fruit using allyl isothiocyanate encapsulated by electrospun zein ultrafine fibers. LWT - Food Science and Technology 143: 111087 (2021)

Dissa AO, Desmorieux H, Bathiebo J, Koulidiati J. Convective drying characteristics of Amelie mango (*Mangifera Indica* L. cv. 'Amelie') with correction for shrinkage. Journal of Food Engineering 88: 429-437(2008)

Gaware TJ, Sutar N, Thorat BN. Drying of tomato using different methods: Comparison of dehydration and rehydration kinetics. Drying Technology 28: 651-658 (2010)

Gol NB, Patel PR, Rao TVR. Improvement of quality and shelf-life of strawberries with edible coatings enriched with chitosan. Postharvest Biology and Technology 85: 185-195 (2013)

Guerreiro AC, Gago CML, Faleiro ML, Miguel MGC, Antunes MDC. Raspberry fresh fruit quality as affected by pectin- and alginate-based edible coatings enriched with essential oils. Scientia Horticulturae 194: 138-146 (2015)

Henderson SM, Pabis S. Grain drying theory: Temperature effect on drying coefficient. Journal of Agricultural Engineering Research 6: 169-174 (1961)

Huang D, Yang P, Tang X, Luo L, Sunden B. Application of infrared radiation in the drying of food products. Trends in Food Science and Technology 110: 765-777 (2021)

Iguaz, A., San Martín MB, Matíe JI, Fernandez T, Vírseda P. Modelling effective moisture difusivity of rough rice (*Lido* cultivar) at low drying temperatures. Journal of Food Engineering 59: 253-258 (2003)

Jain D, Pathare PB. Selection and evaluation of thin layer drying models for infrared radiative and convective drying of onion slices. Biosystems Engineering 89(3): 289-296 (2004)

Jamradloedluk J, Nathakaranakule A, Soponronnarit S, Prachayawarakorm S. Influences of drying medium and temperature on drying kinetics and quality attributes of durian chip. Journal of Food Engineering 78: 198-205 (2007)

Jiang N, Liu C, Li D, Zhang Z, Liu C, Wang D, Niu L, Zhang M. Evaluation of freeze drying combined with microwave vacuum drying for functional okra snacks: Antioxidant properties,

sensory quality, and energy consumption. LWT - Food Science and Technology 82: 216-226 (2017)
Khampakool A, Soisungwan S, You S, Park SH. Infrared assisted freeze-drying (IRAFD) to produce shelf-stable insect food from *Protaetia brevitarsis* (white-spotted flower chafer) larva. Food Science of Animal Resources 40(5): 813-830 (2020)
Khampakool A, Soisungwan S, Park SH. Potential application of infrared assisted freeze drying (IRAFD) for banana snacks: Drying kinetics, energy consumption, and texture. LWT-Food Science and Technology 99: 355-363 (2019)
Krokida MK, Philippopoulos C. Rehydration of dehydrated foods. Drying Technology 23: 799-830 (2005).
Kumar C, Karim MA, Joardder MUH. Intermittent drying of food products: A critical review. Journal of Food Engineering 121: 48-57 (2014)
Lin YP, Tsen JH, King VAE. Effects of far-infrared radiation on the freeze-drying of sweet potato. Journal of Food Engineering 68: 249-255 (2005)
Liu W, Zhang M, Adhikari B, Chen J. A novel strategy for improving drying efficiency and quality of cream mushroom soup based on microwave pre-gelatinization and infrared freeze-drying. Innovative Food Science and Emerging Technologies 66: 102516 (2020)
Lopez-Quiroga E, Prosapio V, Fryer PJ, Norton IT, Bakalis S. Model discrimination for drying and rehydration kinetics of freeze-dried tomatoes. Journal of Food Process Engineering 43: e13192 (2020)
Maskan A, Kaya S, Maskan M. Hot air and sun drying of grape leather (pestil). Journal of Food Engineering 54: 81-88 (2002)
Merone D, Colucci D, Fissore D, Sanjuan N, Carcel JA. Energy and environmental analysis of ultrasound-assisted atmospheric freeze-drying of food. Journal of Food Engineering 283: 110031 (2020)
Monteiro RL, Link JV, Tribuzi G, Carciofi BAM, Laurindo JB. Effect of multi-flash drying and microwave vacuum drying on the microstructure and texture of pumpkin slices. LWT - Food Science and Technology 96: 612–619 (2018)
Pan Z, Shih C, McHugh TH, Hirschberg E. Study of banana dehydration using sequential infrared radiation heating and freeze-drying. LWT - Food Science and Technology 41: 1944-1951 (2008)
Park SH, Balasubramaniam VM, Sastry SK, Lee J. Pressure–ohmic–thermal sterilization: A feasible approach for the inactivation of *Bacillus amyloliquefaciens* and *Geobacillus stearothermophilus* spores. Innovative Food Science and Emerging Technologies 19: 115-123 (2013)
Park SH, Balasubramaniam VM, Sastry SK. Quality of shelf-stable low-acid vegetables processed using pressure-ohmic-thermal sterilization. LWT - Food Science and Technology 57: 243-252 (2014)
Park SH, Jo YJ. Static hydrothermal processing and fractionation for production of a collagen peptide with anti-oxidative and anti-aging properties. Process Biochemistry 83: 176-182 (2019)
Pawar SB, Pratape VM. Fundamentals of infrared heating and its application in drying of food materials: A Review. Journal of Food Process Engineering 40: e12308 (2017)
Potter R, Stojceska V, Plunkett A. The use of fruit powders in extruded snacks suitable for children's diets. LWT - Food Science and Technology 51: 537-544 (2013)
Roe LS, Meengs JS, Birch LL, Rolls BJ. Serving a variety of vegetables and fruit as a snack increased intake in preschool children[1,2,3]. The American Journal of Clinical Nutrition 98(3): 693-699 (2013)
Sakare P, Prasad N, Thombare N, Singh R, Sharma SC. Infrared drying of food materials: Recent Advances. Food Engineering Reviews 12: 381-398 (2020)
Senadeera W, Bhandari BR, Young G, Wijesinghe B. Influence of shapes of selected vegetable materials on drying kinetics during fluidized bed drying. Journal of Food Engineering 58: 277-283 (2003)
Shih C, Pan Z, McHugh T, Wood D, Hirschberg E. Sequential infrared radiation and freeze-drying method for producing crispy strawberries. American Society of Agricultural and Biological Engineers 51(1): 205-216 (2008)
Simal S, Femenia A, Garau MC, Rosselló C. Use of exponential, Page's and diffusional models to simulate the drying kinetics of kiwi fruit. Journal of Food Engineering 66: 323-328 (2005)
Temiz NN, Özdemir KS. Microbiological and physicochemical quality of strawberries (*Fragaria ×ananassa*) coated with *Lactobacillus rhamnosus* and inulin enriched gelatin films. Postharvest Biology and Technology 173: 111433 (2021)
Van De Velde F, Tarola AM, Güemes D, Pirovani ME. Bioactive compounds and antioxidant capacity of Camarosa and Selva strawberries (*Fragaria x ananassa* Duch.). Foods 2(2): 120-131 (2013)
Wang R, Zhang M, Mujumdar AS. Effect of food ingredient on microwave freeze drying of instant vegetable soup. LWT - Food Science and Technology 43: 1144-1150 (2010)
Wu XF, Zhang M, Bhandari B. A novel infrared freeze drying (IRFD) technology to lower the energy consumption and keep the quality of *Cordyceps militaris*. Innovative Food Science and Emerging Technologies 54: 34-42 (2019a)
Wu XF, Zhang M, Bhandari B, Li Z. Effects of microwave assisted pulse fluidized bed freeze-drying (MPFFD) on quality attributes of *Cordyceps militaris*. Food Bioscience 28: 7-14 (2019b)
Yeganehzad S, Kiumarsi M, Nadali N, Rabie Ashkezary M. Formulation, development and characterization of a novel functional fruit snack based on fig (*Ficus carica L.*) coated with sugar-free chocolate. Heliyon 6: e043502 (2020)
Zdunkowski W, Bott A. Thermodynamics of the atmosphere. Cambridge University, Cambridge, UK. pp. 33-37 (2004)
Zhang L, Qiao Y, Wang C, Liao L, Shi D, An K, Hu J, Wang J, Shi L. Influence of high hydrostatic pressure pretreatment on properties of vacuum-freeze dried strawberry slices. Food Chemistry 331: 127203 (2020a)
Zhang L, Liao L, Qiao Y, Wang C, Shi D, An K, Hu J. Effects of ultrahigh pressure and ultrasound pretreatments on properties of strawberry chips prepared by vacuum-freeze drying. Food Chemistry 303: 125386 (2020b)
Zhang M, Tang J, Mujumdar AS, Wang S. Trends in microwave related drying of fruits and vegetables. Trends in Food Science and Technology 17: 524-534 (2006)